ACTA IMEKO
ISSN: 221-870X
December 2020, Volume 9, Number 5, 394-400

Dynamic Calibration of Digital Angular Rate Sensors

B. Seeger[1], L. Klaus[1], and D. Nordmann[1]

[1]Physikalisch-Technische Bundesanstalt, Braunschweig und Berlin, Germany, benedikt.seeger@ptb.de
[1]Physikalisch-Technische Bundesanstalt, Braunschweig und Berlin, Germany, leonard.klaus@ptb.de
[1]Physikalisch-Technische Bundesanstalt, Braunschweig und Berlin, Germany, denis.nordmann@ptb.de

Abstract

MEMS gyroscopes / angular rate sensors are often equipped with a digital output only. As part of a European research project, the dynamic calibration of sensors with digital output is being investigated. In the following, the operation principle of digital gyroscopes is described, a possible way to derive correct timestamped data from those sensors using a digital acquisition unit is explained and a calibration procedure is presented. The calibration of the analogue input of the digital acquisition unit, which is a prerequisite to derive correct phase responses, is described. Measurements with digital sensors proved the working principles and gave insight into the dynamic behaviour of those gyroscopes.

1 INTRODUCTION

In order to dynamically calibrate a sensor, precise knowledge of the time relationship between the data of the sensor and the reference system is necessary. This is normally achieved by synchronous sampling.

1.1 Digital Sensors

In contrast to classical analogue gyroscopes and accelerometers, analogue to digital conversion (ADC) takes place completely within the "digital" sensor. There is generally no way to access the analogue signals. In the following, sensors with digital-only interfaces are called *digital sensors* for simplicity. The sampling clock of digital sensors is usually generated by the MEMS (micro-electro-mechanical system) sensor itself and cannot be read or fed from the outside.

In a typical implementation an interrupt signal is issued after the internal signal acquisition is carried out and the data processing is complete. The data then can be transferred from the sensor to a (micro-)computer system for further processing.

1.2 MEMS Gyroscopes

Figure 1 schematically shows the design of a digital tuning fork MEMS gyroscope. To read data from such a sensor, the sensor's settings are programmed via the communication interface (blue). After programming the parameters, such as sampling rate (green), sensitivity and digital filter settings (yellow), the sensor continuously acquires data. If a set of measured values is ready to be read out via the digital interface, the sensor signals this by issuing an interrupt signal. Usually there is only one interrupt for all measuring channels (this example has three), so the exact time delay between data acquisition and the interrupt will be part of the phase response derived by the calibration.

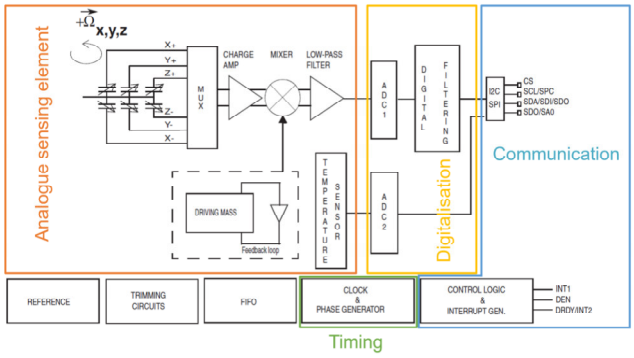

Figure 1: Block diagrame of a tuning fork MEMS gyroscope with functional blocks. No signals can be read directly from the analogue section marked in orange. The ADC cannot be triggered externally. This diagramme is modified from [1].

2 CALIBRATION OF DIGITAL SENSORS

To adress this issue that no direct access to the analogue part of a digital sensor is possible, it is necessary to assess the timing behaviour of such a sensor.

2.1 The Data Acquisition Unit

This was carried out by developing a data acquisition unit (DAU) which connects to the sensor to derive the data points and timestamp these, while synchronously sampling an analogue reference voltage (which is timestamped as well). By timestamping each interrupt corresponding to a set of reference data, the possible asynchronism and fluctuations of the MEMS sample clock can be taken into account when calibrat-

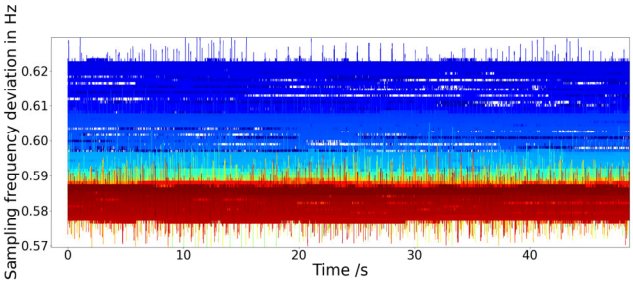

Figure 2: The deviation of the actual sample rate from the nominal value is shown. For each specimen (red first, and blue last). Both, short term jitter effects, e.g. spikes, as well as a continuous drift over time can be found.

ing this kind of sensor [2].The data acquisition is carried out using a self-developed open source data acquisition unit (DAU) based on a STM32 microcontroller[1] [2, 3, 4]. The microcontroller system has a satellite-based time base. The DAU also has analogue inputs which are hardware synchronised to the time-stamped interrupt signals.

2.2 *Absolute Timestamping*

The oscillators used in these inexpensive and very small sensors are imprecise and can undergo significant changes during operation. An independent and precise clock is a prerequisite to analyse these effects. The satellite-based reference clock in the DAU allows the timestamping of digital samples and the analogue reference voltage with 200 ns uncertainty.

Figure 2 shows the deviation of the sampling frequency of a typical sensor from the nominal value during a calibration run of about 4 h. The sampling frequency f_{sample} is calculated as the inverse of the time difference between two consecutive samples. The sampling frequency deviates from the nominal value up to 390 ppm during the measurements. For sensors whose internal clock generation is not based on a MEMS oscillator (as in the case of the sensor shown here) but on RC oscillators, these fluctuations can be in the order of whole percentages. Therefore, the assumption that the sampling rate is constant and has a negligible influence on the measurement is no longer justifiable. When using Fourier-based methods, interpolation to equidistant samples is therefore advisable. The three- and four-parameter sinus approximations used in this article do not demand equidistant samples and therefore do not require interpolation.

[1]Commercial components are identified in this paper only to adequately specify the experimental set-up. Such identification does not imply recommendation by PTB, nor does it imply that the equipment identified is necessarily the best available for the purpose.

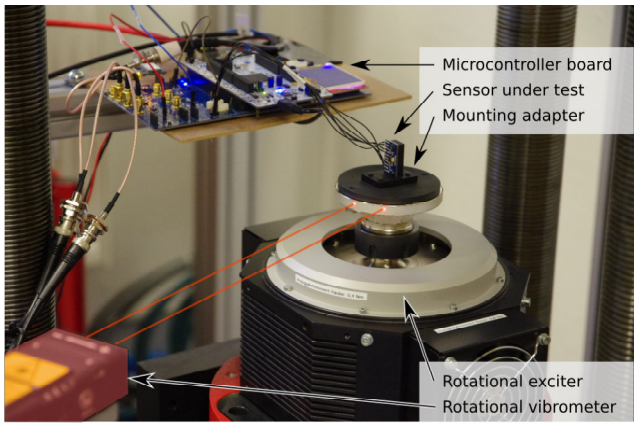

Figure 3: Calibration set-up consisting of the microcontroller board (DAU), the device under test, the rotational exciter and the rotational laser vibrometer as reference (laser beams and housing are highlighted in red). In this configuration the X-axis of the sensor is excited.

3 CALIBRATION SET-UP

The calibration set-up consists of a mechanical exciter to generate the oscillations which then, are measured by the sensor under test and a reference. The data acquisition is divided into the classic, analogue data acquisition with precise digitisers to acquire the reference signal and into the data acquisition unit which reads out the digital sensor data.

3.1 *Exciter*

The calibration set-up used for these investigations is based on a rotational exciter manufractured by Acutronic (type 170.01). This exciter generates sinusoidal excitations in a frequency range from DC (constant rotation) up to about 1 kHz. An assembly of components mounted to the exciter gives the surface for the reference angular velocity measurement and enables the transducerto be mounted in different positions, to excite each of the three measurement axes, respectively. The set-up is depicted in Figure 3.

3.2 *Traceability*

The traceability of the calibration is realised by using a rotational laser vibrometer (Polytec RLV-5500) as reference. The analogue voltage output of the vibrometer is proportional to the measured angular velocity. The analogue output was calibrated on one of PTB's primary angular acceleration standards in the past. This makes the calibration of the digital gyroscope a secondary calibration.

The voltage output of the rotational laser vibrometer is acquired by a high-precision digitiser card manufactured by National Instruments. The analogue inputs are again calibrated traceable to the national standards. For the calibration of the sensor, the independent data

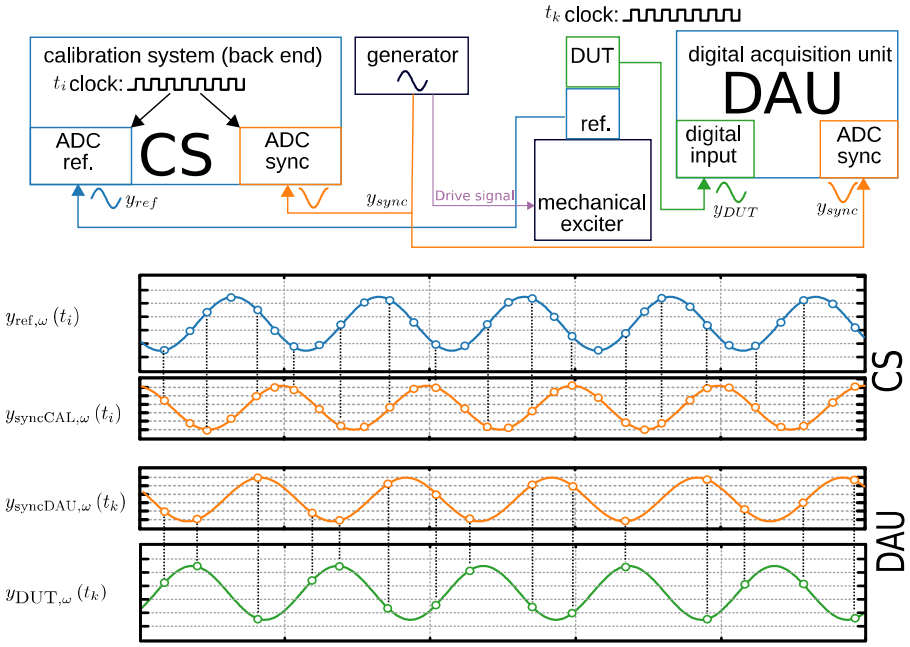

Figure 4: The analogue calibration system (CS) with the digital acquisition unit (DAU) and a MEMS sensor attached. The DAU samples data from the MEMS sensor y_{DUT} an constant amplitude synchronisation signal y_{syncDAU} is sampled at the same time. The existing analogue calibration system samples the reference signal y_{ref} and the synchronisation signal y_{syncCAL} simultaniosly [2]. All signals witch are phase synchronous to the mechanical excitation and have sufficient peak-to-peak amplitude ($>100\,\mathrm{mV_{pp}}$) can be used as synchronisation signals, e.g. reference sensor signals, excitation signals, or, as in the set-up presented here, a constant amplitude synchronisation signal from the generator.

acquisition of the MEMS sensor's output and the acquisition of the analogue angular velocity signal are synchronised by using a common analogue signal acquired by a second channel of the precision digitiser and an analogue input on the microcontroller board.

Figure 4 shows the different sampled signals and their relations. The phase relationship between the digital and analogue calibration system can be calibrated, since the synchronisation signal y_{sync} is sampled by the DAU and by the analogue calibration system (denoted y_{syncDAU} and y_{syncCAL}, respectively). The phase delay between the DUT (y_{DUT}) and the reference (y_{Ref}) can be calibrated with this link. The magnitude response can be derived directly from y_{REF} and y_{DUT}. The phase response $\Delta\varphi(\omega)$ is given by

$$|S(\omega)| = \frac{\widehat{Y}_{\mathrm{DUT}}(\omega)}{\widehat{Y}_{\mathrm{ref}}(\omega)} \quad \text{and} \tag{1}$$

$$\Delta\varphi(\omega) = \left(\varphi_{\mathrm{DUT}}(\omega) - \varphi_{\mathrm{syncDAU}}(\omega) - \Delta\varphi_{DAUADC}(\omega)\right) - \left(\varphi_{\mathrm{ref}}(\omega) - \varphi_{\mathrm{syncCAL}}(\omega)\right). \tag{2}$$

3.3 *Analogue Calibration of the Data Acquisition Unit*

One analogue input of the data acquisition unit is used to determine the initial phase delay $\varphi_{\mathrm{syncDAU}}$. Therefore, the transfer function of this input needs to be known. The analogue input is calibrated with reference to the DAU's time base using a two-channel function generator (Rigol DG 4062). One channel of the function generator is configured to generate a square wave train with a constant frequency f_{sample}(e.g. 999 Hz) and a number of cycles n which are used to trigger the analogue-to-digital conversion at times ($t_i = t_1, t_2, \ldots t_n$). All properties of this channel are denoted with the index *sample*. The second channel of the function generator is configured to generate an analogue sine signal giving

$$y[t_i] = \hat{A}_{\mathrm{cal}} \cdot \sin(2\pi \cdot f_{\mathrm{cal}} \cdot t_i + \varphi_{\mathrm{cal}}) \tag{3}$$

with the excitation frequency f_{cal} (e.g. 1000 Hz) and the same initial phase ($\varphi_{\mathrm{cal}} = \varphi_{\mathrm{sample}} = 0$) as the first channel with the square-wave output. A sequential four-parameter IEEE-STD-1057 sine approximation [5] is applied to the absolute timestamped analogue values $Y_{\mathrm{ADC}}[t_{\mathrm{ADC}}]$. It provides the parameters frequency ($f_{\mathrm{ADCCalFit}}$), amplitude ($\hat{A}_{\mathrm{ADC}}$), phase angle (φ_{ADC}), and offset (C_{ADC}) as follows

$$y_{\mathrm{DAUADC}}[t_{\mathrm{ADC}}] \approx \hat{A}_{\mathrm{ADC}} \cdot \sin(2\pi \cdot f_{\mathrm{ADCCalFit}} \cdot t_{\mathrm{ADC}} + \varphi_{\mathrm{ADC}}) + C_{\mathrm{ADC}} \quad . \tag{4}$$

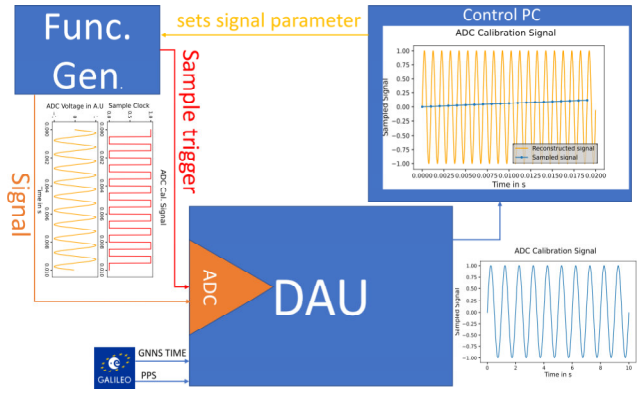

Figure 5: Calibration of the data acquisition unit's analogue input with a 1000 Hz test signal at 999 Hz sample clock. This results in an apparent 1 Hz signal in the time stamped ADC data, from which the 1000 Hz signal can be reconstructed with knowledge of the actual test frequency.

The amplitude and phase response of the analogue input can then be determined by the following equations:

$$|S_{\mathrm{DAUADC}}(f_{\mathrm{ADCCal}})| = \frac{\hat{A}_{\mathrm{ADC}}(f_{\mathrm{ADCCal}})}{\hat{A}_{\mathrm{ADCNominal}}(f_{\mathrm{ADCCal}})} \quad \text{and} \tag{5}$$

$$\Delta\varphi_{\mathrm{DAUADC}}(f_{\mathrm{ADCCal}}) = \varphi_{\mathrm{ADC}}(f_{\mathrm{ADCCal}}). \tag{6}$$

Hence the timestamps generated by the DAU are used as time base for the sine approximation. Distortions (drift, jitter) resulting from this time base are included in this calibration. This calibration method is essentially identical to measurements with equivalent time subsampling, so frequencies f_{ADCCal} above the sampling frequency $f_{\mathrm{ADCSample}}$ can also be calibrated. Figure 5 shows a calibration where $f_{\mathrm{ADCCal}} = 1000\,\mathrm{Hz}$ and $f_{\mathrm{ADCSample}} = 999\,\mathrm{Hz}$, resulting in a beat frequency of 1 Hz.

4 CALIBRATION PROCEDURE

The calibration was designed to be carried out automatically, both in terms of the excitation generation and the data acquisition.

The oscillation is controlled by a commercial control system (DataPhysics SignalStar Scalar), enabling an automatic adjustment of the magnitudes. The excited oscillations are monofrequent sinusoidal excitations which are excited subsequently at different frequencies. Between the different measuring points, the system pauses the excitation for 10 s. The excitation frequencies are given in Table 1. At frequencies above 63 Hz the amplitude is reduced due to the limited angular acceleration capabilities of the exciter.In addition to the drive signal, the control system also generates a phase synchronous voltage output with a constant amplitude of 9.6 V_{pp} (peak-to-peak) which is used as the synchronisation signal y_{sync}.

Table 1: **Calibration results of *sensor 1* of the analysed TDK InvenSense MPU9250 sensors.**

Freq.	**Exc. level**	**Mag. res.**	**Mag. res. uncer.**	**Phase res.**	**Phase res. uncer.**	**Phase delay**
f Hz	deg/s	$\lvert S_x \rvert$	%	$\Delta\varphi_x$ deg	deg	τ ms
4	200	1.000	0.09	-3.23	0.03	2.25
5	200	1.000	0.08	-4.09	0.03	2.27
6.3	200	1.000	0.08	-5.22	0.08	2.3
8	200	1.000	0.08	-6.74	0.16	2.34
10	200	1.000	0.10	-8.42	0.19	2.34
12.5	200	1.000	0.09	-10.5	0.21	2.34
16	200	1.000	0.11	-13.4	0.23	2.32
20	200	1.000	0.12	-16.6	0.23	2.31
25	200	0.999	0.11	-20.8	0.25	2.31
31.5	200	0.997	0.11	-26.1	0.26	2.3
40	200	0.993	0.15	-33.0	0.22	2.29
50	200	0.987	0.15	-41.0	0.09	2.28
63	200	0.978	0.22	-51.5	0.06	2.27
80	159	0.964	0.22	-65.9	0.10	2.29
100	127	0.943	0.21	-83.1	0.09	2.31
125	102	0.899	0.45	-105	0.07	2.34
160	79.4	0.799	0.36	-139	0.06	2.41
200	63.5	0.617	0.64	-177	0.04	2.45
250	50.8	0.383	0.67	-217	0.03	2.41

The data acquisition unit, as well as the data acquisition system, continuously acquires data until stopped.

4.1 Data Analysis

During calibration, two data files containing the time series of the digital sensor and of the calibration system are generated. The data is stored in one long time series. In order to determine the transfer function of the device under test, the time series needs to be divided into sections of valid measurement data. Each cut-out should contain valid data of one excitation frequency.

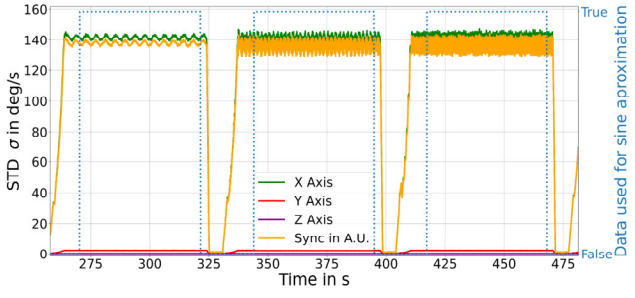

Figure 6: The block-wise standard deviation of the signal amplitude of the signals recorded by the DAU during the calibration run for three frequencies is shown. The sin approximation is performed for the data marked as valid. The ripple of σ is caused by different inertial phases of the signal in each block.

To process the data automatically, we made use of the fact that between each excitation frequency, the excitation was paused for 10 s and ramped up afterwards. To determine which data is valid, the standard deviation of n (e.g. 128) consecutive samples is calculated throughout the time series. For pure sine signals, the standard deviation (σ) and the signal amplitude ($\hat{A}$) are linked giving

$$\sigma = \frac{\hat{A}}{\sqrt{2}} \quad . \tag{7}$$

If σ is above a threshold value (e.g. 20 % of the smallest excitation level in the measurement) for a certain amount of those n-sample blocks (e.g. $100 \cdot 128$ samples ≈ 12.8 s), the data after these blocks will be defined as valid measurement data until the criteria is not met any more. Finally, at the end of this identified valid data, a certain amount of samples (e.g. $30 \cdot 128$ samples ≈ 3.84 s) is removed to ensure that the ramp down for the 10 s pause is not present in the data used for the calibration.

This calculation is carried out for the whole dataset, giving blocks of valid data for the different excitation frequencies. Figure 6 shows a time series with three extracted blocks of valid data. In the figure the invalid data at the beginning of the time series is rougly three times longer than at the end.

For each block of valid data, the initial values for a four-parameter IEEE-STD-1057 sine approximation are obtained by means of a discrete fourier transform. Based on the excitation frequency determined by the four-parameter approximation, the signal's amplitudes $\hat{Y}_{\mathrm{DUT}}(\omega)$ and initial phases $\varphi_{\mathrm{DUT}}(\omega)$ are determined by sequential three-parameter sine approximation.

5 MEASUREMENT RESULTS

To assess the developed calibration procedure, measurements with two sensors were carried out.

5.1 Magnitude and Phase Response

The calibration was carried using an MPU9250 sensor from TDK InvenSense. This sensor is designed as an inertial measuring unit and can therefore measure angular velocity, acceleration, magnetic flux density and temperature. The sensor was calibrated with a set data rate of 1000 S/s in a measuring range of ± 2000 deg/s. The obligatory digital low pass in the sensor was configured to a bandwidth of 184 Hz. Two different sensors were used for the measurements. They where denoted as *sensor 1* and *sensor 2*, respectively.

The calibration results for *sensor 1* are given in Table 1 and in Fig. 7. As can be seen in the results, the sensor shows a distinctive low pass behaviour. Before the magnitude response drops to the higher frequency, a constant transfer function can be found up to 50 Hz/63 Hz. The previously described low-pass filter frequency is well within the excitation frequency. The corresponding phase delay τ can be calculated (cf. the last column in Table 1) from the phase response data. The overall stable number indicates that the dominant factor in the phase response might be the group delay of the integrated digital low-pass filter which could be in the range of about 2.3 ms.

Figure 7 does not just show one measurement result, but rather 10 repeated measurements without dismounting and remounting the sensor. In the plot it can be seen, that the repeatability under those conditions is very good. Only two frequencies, namely 50 Hz and 100 Hz, show higher deviations, most probably due to the mains frequency of 50 Hz.

5.2 Repeated Measurements

After *sensor 1*, *sensor 2* (of the same type as sensor 1) was also calibrated along both the X- and the Y-Axis. Figures 7 and 9 show the deviations of the amplitudes and phase response from the mean value of all measurements at the different excitation frequencies.

It can be seen that the measurements for an axis do not always agree within the purely statistical uncertainty contributions as specified in Table 1.

5.3 Uncertainty Contributions

The uncertainty contributions shown here take only statistical information into account. This also applies to the calibration of the analogue input of the DAU and the analogue reference measuring system. These statistical uncertainties were propagated starting with the measurements during the calculation of the transfer coefficients and serve as weighting factors for the final mean value formation taken form the repeat measurements. Figure 10 shows the yet identified sources of uncertainty, the influences marked in green are likely to lead to statistical influences and are therefore covered, the influences marked in blue are either static or have long-term impact and are therefore not yet covered (sutch as the temperature and mechanical effects).Althrough the circuit boards on which the sensors are mounted have comparably high tolerances, no alignment pins or similar tools for a precise alignment exist. This can lead to the axis under investigation not being perfectly aligned with the axis of excitation, which results in amplitude deviations. The phase deviations could be caused by mechanical hysteresis effects.

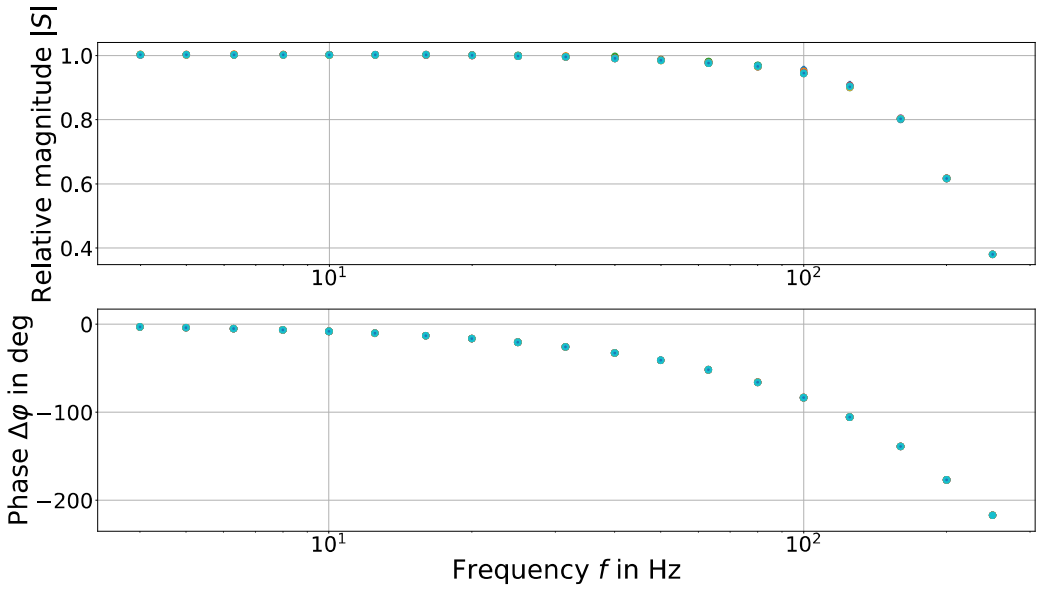

Figure 7: Transfer function for excitation along the X axis for *sensor 1* of the analysed MPU9250 sensors. The constant group delay of the digital low-pass filter of about 2.3 ms can be seen in the phase response.

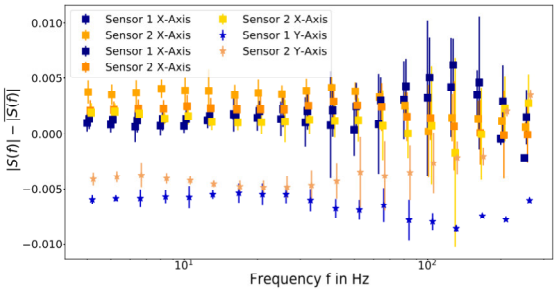

Figure 8: The calibration measurements were performed several times for the X- and Y-Axis with 2 different sensors. Each series of measurements contains ten repetitions. A small frequency shift was added later for better visualisation.

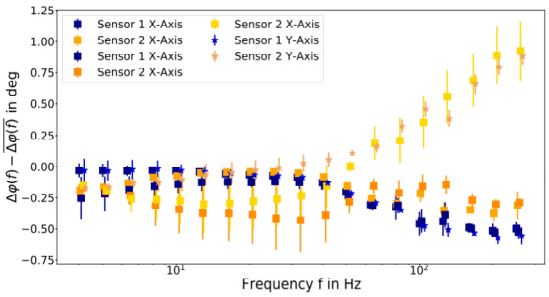

Figure 9: The calibration measurements were performed several times for the X- and Y-Axis with 2 different sensors. Each series of measurements contains ten repetitions. A small frequency shift was added later for better visualisation.

6 SUMMARY AND OUTLOOK

The methodology shown here can be used to dynamically calibrate gyroscopes and accelerometers with exclusively digital data output by magnitude and phase. By using a synchronisation between the digital acquisition unit and the existing analogue calibration system, no modifications are necessary with the latter. The digital sensor's data is timestamped and processed in a digital acquisition unit which also acquires an analogue synchronisation signal. The calibration of the analogue input is also described in this paper. The calibration system used here enables angular velocity calibrations with amplitudes up to 200 deg/s traceable to the national standards by means of a rotational vibrometer.

Automatic data analysis helps to split the acquired time series data into data blocks with valid data. The transfer function of the device under test is derived by successive sine approximations according to IEEE 1057.

The Measurement results of a calibration of two TDK InvenSense MPU9250 sensors show good repeatability of the results. The derived magnitude and phase response functions seem dependable. The phase response of this type of sensor is dominated by the group delay of the integrated digital low pass filter.

However, it was found that significant deviation occurs after dismounting and mounting a sensor. The reproducibility seems to be limited by mechanical alignment. The set-up can be modified with alignment pins or similar to improve the situation, but the limited precision of the circuit boards will remain.

For the final estimation of the measurement uncertainties, it is necessery to extend the effects that are taken into account to include all the relevant effects. Up to now, only statistical contributions are covered.

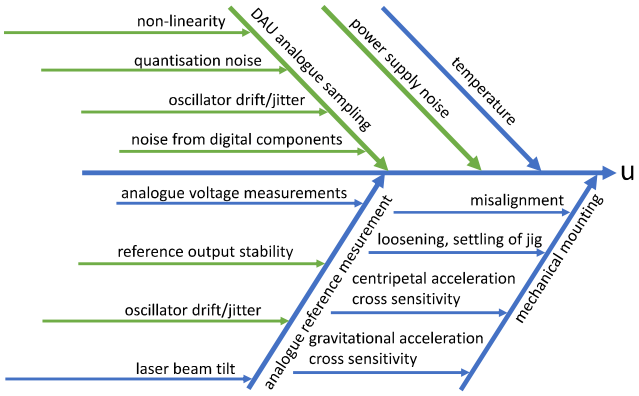

Figure 10: Overview of the potential uncertainty contributions on the sensor calibration.The only green influences are covered by the statistical methods used so far.

ACKNOWLEDGMENTS

This work is part of the Joint Research Project 17IND12 *Metrology for the Factory of the Future (Met4FoF)* of the European Metrology Programme for Innovation and Research (EMPIR). The EMPIR is jointly funded by the EMPIR participating countries within EURAMET and the European Union.

7 References

[1] STMicroelectronics 2013 *L3GD20H MEMS motion sensor: three-axis digital output gyroscope* URL `https://www.st.com/resource/en/datasheet/l3gd20h.pdf`

[2] Seeger B, Bruns T and Eichstädt S 2019 Methods for dynamic calibration and augmentation of digital acceleration mems sensors. *19th International Congress of Metrology (CIM2019)* (EDP Sciences) p 22003

[3] Seeger B Github.com:met4fof/met4fof-smartupunit `https://github.com/Met4FoF/Met4FoF-SmartUpUnit`

[4] Seeger B circuitmaker.com:met4fof interface board `https://workspace.circuitmaker.com/Projects/Details/Benedikt-Seeger-2/Met4FoF-Interface-Board`

[5] Händel P 2000 *IEEE Transactions on Instrumentation and Measurement* **49** 1189–1193